

Personalized Rehabilitation Robotics based on Online Learning Control

Samuel Tesfazgi^{1*}, Armin Lederer^{1*}, Johannes F. Kunz, Alejandro J. Ordóñez Conejo, Sandra Hirche¹

Abstract— The use of rehabilitation robotics in clinical applications gains increasing importance, due to therapeutic benefits and the ability to alleviate labor-intensive works. However, their practical utility is dependent on the deployment of appropriate control algorithms, which adapt the level of task-assistance according to each individual patient’s need. Generally, the required personalization is achieved through manual tuning by clinicians, which is cumbersome and error-prone. In this work we propose a novel online learning control architecture, which is able to personalize the control force at run time to each individual user. To this end, we deploy Gaussian process-based online learning with previously unseen prediction and update rates. Finally, we evaluate our method in an experimental user study, where the learning controller is shown to provide personalized control, while also obtaining safe interaction forces.

I. INTRODUCTION

In recent years neurological disorders have become more dominant with an estimate of over 16 million people suffering a first stroke each year [1]. Therefore, an urgent need for rehabilitation treatments arises to ensure the quality of living for such patients. In particular high-intensity and repetition training has been shown to produce the most promising recovery results [2]. Due to these requirements, effective rehabilitation is labor intensive and both patients and healthcare professionals can benefit greatly from robotic-assisted rehabilitation strategies [3]. However, the control of these devices presents certain challenges, which can limit their applicability in practice. Different factors, such as level of assistance, patient engagement and task success, have to be considered when designing the controller. These requirements are particularly difficult to fulfill, due to the uncertain interaction dynamics between human and robot. This problem is exacerbated by the variety of patient behaviors and needs, which require a high degree of personalization.

A control approach that is widely used in the literature is impedance control, which has previously been shown to be applicable for robot-based arm rehabilitation [4]. Impedance control is particularly popular for human-robot interaction, since it provides compliant behavior for appropriately chosen parameters, therefore, ensuring limited and safe interaction forces. In [5], a position-dependent stiffness is used to assist rehabilitation tasks, where the stability of the human-robot interaction is guaranteed using system passivity. Differently, in [6], a desired impedance model is defined, which is subsequently achieved through an iterative learning scheme. However, despite these application examples of impedance con-

trol for robot-based neurorehabilitation, they generally hinge on properly chosen impedance parameters, which first have to be tuned by the manufacturer a-priori and are then readjusted by clinicians [5]. This procedure is time-consuming and error prone, due to the variety of target personas. Additionally, the tuning needs to be performed cautiously in order to retain the compliant behavior needed for safe interaction. To address these issues other works have developed control architectures that specifically take the complete dynamics into consideration, e.g., via feed-forward control and disturbance observers [7]. While this approach decreases interaction forces, it requires measurements of the patient-robot interaction wrench at each interaction point, such that undesirable force-torque sensors become necessary, which increase system costs and may even lead to stability concerns [8].

Alternatively, learning-based controllers can be deployed to fulfill the personalization requirements. To deal with the unknown interaction model and to adapt the patient-robot interaction, He et al. [9] propose a neural network control approach for rehabilitation robotics. Differently, the authors in [10] focus on obtaining human motor control models during physical interaction by deploying Gaussian processes (GPs) to learn the human arm impedance. Despite these approaches showing promising results, they cannot account for behavior changes of the patient, i.e., due to fatigue, since the learning is performed offline. However, facilitating this adaptation can be highly beneficial for the personalization of control strategies in rehabilitation robotics [11].

In this work we present a novel learning-based control architecture that facilitates highly personalized assistance in a human-robot collaboration task, while requiring no parameter tuning. To the best of our knowledge, this is the first time that a GP is used directly in the control loop to generate assistive forces during physical human-robot interaction. Additionally, we evaluate our learning-based control architecture experimentally, where update and prediction rates with online-generated data are achieved that are orders of magnitude higher than previous GP approaches. The remainder of the paper is structured as follows: First the problem statement is introduced in Section II, while the online learning approach is presented in Section III. Subsequently, in Section IV, the online learning control architecture is proposed. Finally, the evaluation of our method follows in Section V.

II. PROBLEM FORMULATION

We model the physical-human robot interaction in rehabilitation robotics using Euler-Lagrange systems of the form

$$\mathbf{H}(\mathbf{q})\ddot{\mathbf{q}} + \mathbf{C}(\mathbf{q}, \dot{\mathbf{q}})\dot{\mathbf{q}} + \mathbf{g}(\mathbf{q}) + \mathbf{f}_i(\mathbf{x}) = \mathbf{u}, \quad (1)$$

¹Samuel Tesfazgi, Armin Lederer and Sandra Hirche are with the Chair of Information-oriented Control (ITR), Department of Electrical and Computer Engineering, Technical University of Munich, Germany {armin.lederer, samuel.tesfazgi, hirche}@tum.de

*These authors contributed equally.

where $\mathbf{x} = [\mathbf{q}^T \quad \dot{\mathbf{q}}^T \quad \ddot{\mathbf{q}}^T \quad t]^T$ is the concatenation of joint angles $\mathbf{q} \in \mathbb{R}^d$, angular velocities $\dot{\mathbf{q}} \in \mathbb{R}^d$, angular accelerations $\ddot{\mathbf{q}} \in \mathbb{R}^d$, and the time $t \in \mathbb{R}_{0,+}$. The matrix $\mathbf{H} : \mathbb{R}^d \rightarrow \mathbb{R}^{d \times d}$ denotes the symmetric and positive definite generalized inertia of the robotic system, $\mathbf{C} : \mathbb{R}^d \times \mathbb{R}^d \rightarrow \mathbb{R}^{d \times d}$ is the generalized Coriolis matrix, $\mathbf{g} : \mathbb{R}^d \rightarrow \mathbb{R}^d$ are the torques resulting from gravitation, $\mathbf{f}_i : \mathbb{R}^{3d+1} \rightarrow \mathbb{R}^d$ describes the interaction torques generated by the i -th patient, and $\mathbf{u} \in \mathbb{R}^d$ are torques applied to the system as control input.

Remark 1: We account for the intra-patient variation of interaction dynamics, e.g., caused by unobserved internal dynamics in the patient such as fatigue, by considering time-dependent functions $\mathbf{f}_i(\cdot)$. Hence, all behavioral changes of the human are modeled through time-dependency.

In order to reflect the practical availability of models, we make the following assumption.

Assumption 1: All parameters of the robotic system are known, hence, $\mathbf{H}(\cdot)$, $\mathbf{C}(\cdot, \cdot)$ and $\mathbf{g}(\cdot)$ are available. In contrast, the individual dynamics of patients $\mathbf{f}_i(\cdot)$ are unknown.

This assumption reflects the fact that accurate models of robotic systems can typically be obtained using classical identification procedures [12], which can be directly applied in control design. In contrast, the identification of models of human motor dynamics in physical interaction is a challenging problem and often limited to simple scenarios [10], making them generally inapplicable in rehabilitation robotics.

In order to overcome these limitations of conventional modeling techniques, we employ a non-parametric, data-driven approach for learning the human induced dynamics $\mathbf{f}_i(\cdot)$. For the inference of an individual model for each patient, we consider access to the following measurements.

Assumption 2: The control input \mathbf{u} , the joint angles \mathbf{q} , and the angular velocities $\dot{\mathbf{q}}$ and accelerations $\ddot{\mathbf{q}}$ of each patient can be observed for learning a personalized model.

As the control input \mathbf{u} is determined by the employed control law, it can be directly observed. The joint angles \mathbf{q} are usually measured, such that the angular velocities $\dot{\mathbf{q}}$ and accelerations $\ddot{\mathbf{q}}$ can be obtained through numerical differentiation. It is important to note that we do not require force torque sensors to determine interaction forces, which often suffer from high measurement noise and are expensive.

The task of each patient is the execution of a rehabilitation exercise described by a reference trajectory \mathbf{q}_{ref} for system (1), for which we require the following property.

Assumption 3: The bounded reference trajectory \mathbf{q}_{ref} is twice continuously differentiable with bounded derivatives.

Since abrupt movements must be avoided in physical human-robot interaction, in particular when dealing with impaired patients, the required smoothness of the reference is a natural assumption. Moreover, the assumed boundedness of reference trajectories directly follows from the compact work spaces robots and humans operate in, such that Assumption 3 is not restrictive in practice.

In order to execute the task by tracking the reference trajectory with the human-robot system (1), a control law needs to be defined to determine the control inputs \mathbf{u} . On the one hand, the applicability in real-world rehabilitation robotic

scenarios requires this control law to ensure safe interaction forces by avoiding excessively high control inputs \mathbf{u} . On the other hand, the successful execution of the rehabilitation exercise requires a satisfactory tracking accuracy. These requirements generally pose conflicting goals, which must be traded-off in a control gain tuning phase. However, this tuning process cannot be performed for each patient individually, such that control gains must be employed, which are expected to perform well on a wide range of patients, but can yield rather poor performance for some of them. In order to overcome this issue, we consider the problem of designing a control law which adapts online to the observed behavior of individual patients using non-parameteric machine learning, such that a highly personalized treatment can be realized.

III. GAUSSIAN PROCESS-BASED ONLINE LEARNING

In order to develop control laws achieving the posed design goals, we employ Gaussian process-based machine learning to infer a model of the human motor behavior. The foundations of Gaussian process regression are introduced in Section III-A, before a Gaussian process based online learning algorithm relying on the aggregation of local Gaussian process models is presented in Section III-B.

A. Gaussian Process Regression

Gaussian process (GP) regression bases on the assumption that any finite number of evaluations $\{f(\mathbf{x}^{(n)})\}_{n=1}^N$ of a scalar function $f : \mathbb{R}^\rho \rightarrow \mathbb{R}$, $\rho \in \mathbb{N}$, at inputs $\mathbf{x}^{(n)} \in \mathbb{R}^\rho$ follows a joint Gaussian distribution [13]. This distribution, denoted as $\mathcal{GP}(m(\mathbf{x}), k(\mathbf{x}, \mathbf{x}'))$, is defined in terms of a prior mean function $m : \mathbb{R}^\rho \rightarrow \mathbb{R}$, which can be used to incorporate prior knowledge such as parametric models, and a covariance function $k : \mathbb{R}^\rho \times \mathbb{R}^\rho \rightarrow \mathbb{R}$, capturing more abstract information such as differentiability or periodicity of $f(\cdot)$. If no specific knowledge about the unknown function $f(\cdot)$ is available, $m(\cdot)$ is commonly set to 0, which we also assume in the remainder of the work. The most frequently used covariance function is the squared exponential kernel

$$k(\mathbf{x}, \mathbf{x}') = \sigma_f^2 \exp \left(- \sum_{i=1}^{\rho} \frac{(x_i - x'_i)^2}{2l_i^2} \right), \quad (2)$$

whose shape depends on the signal standard deviation $\sigma_f \in \mathbb{R}_+$ and the length scales $l_i \in \mathbb{R}_+$. The signal standard deviation σ_f and the kernel length scales l_i , $i = 1, \dots, \rho$, form the hyperparameters $\boldsymbol{\theta} = [\sigma_f \quad l_1 \quad \dots \quad l_\rho \quad \sigma_{\text{on}}]^T$ together with an assumed target noise standard deviation $\sigma_{\text{on}} \in \mathbb{R}_+$. The hyperparameters $\boldsymbol{\theta}$ are commonly obtained by maximizing the log-likelihood

$$\begin{aligned} \log p(\mathbf{y} | \mathbf{X}, \boldsymbol{\theta}) = & -\frac{1}{2} \mathbf{y}^T (\mathbf{K} + \sigma_{\text{on}}^2 \mathbf{I}_N)^{-1} \mathbf{y} \\ & - \frac{1}{2} \log(\det(\mathbf{K} + \sigma_{\text{on}}^2 \mathbf{I}_N)) - \frac{n}{2} \log(2\pi), \end{aligned} \quad (3)$$

where we define the elements of the kernel matrix $\mathbf{K} \in \mathbb{R}^{N \times N}$ as $K_{i,j} = k(\mathbf{x}^{(i)}, \mathbf{x}^{(j)})$, and concatenate the training inputs and targets into $\mathbf{X} = [\mathbf{x}^{(1)} \quad \dots \quad \mathbf{x}^{(N)}]^T$ and $\mathbf{y} =$

$[y^{(1)} \dots y^{(N)}]^T$, respectively. Although this maximization involves a non-convex optimization problem, it is typically solved using gradient based optimization methods [13].

After the hyperparameters have been optimized, the posterior distribution can be exactly calculated under the assumption of training targets perturbed by zero mean Gaussian noise with variance σ_{on}^2 . This posterior is again Gaussian with mean and variance

$$\mu(\mathbf{x}) = \mathbf{y}^T (\mathbf{K} + \sigma_{\text{on}}^2 \mathbf{I}_N)^{-1} \mathbf{k}(\mathbf{x}) \quad (4)$$

$$\sigma^2(\mathbf{x}) = k(\mathbf{x}, \mathbf{x}) - \mathbf{k}^T(\mathbf{x}) (\mathbf{K} + \sigma_{\text{on}}^2 \mathbf{I}_N)^{-1} \mathbf{k}(\mathbf{x}), \quad (5)$$

where we define the elements of the kernel vector $\mathbf{k}(\mathbf{x}) \in \mathbb{R}^N$ as $k_i(\mathbf{x}) = k(\mathbf{x}^{(i)}, \mathbf{x})$.

B. Locally Growing Random Trees of Gaussian Processes

When applying Gaussian process regression in a control application, data becomes available sequentially as time proceeds. While Gaussian process regression can be straightforwardly applied to such data streams using rank one updates in principle [14], the computational complexity of this approach scales quadratically with the number of training samples, such that exact inference typically becomes too slow for online learning in control loops.

A common approach in robotics applications to overcome this issue of GPs bases on the divide and conquer principle of splitting up the data set and training multiple local GP models [15]. Locally growing random trees of Gaussian processes (LoG-GPs) are a recently proposed method following this idea, which have been demonstrated to achieve update and prediction rates necessary for online learning within control loops, while preserving many beneficial properties of exact GP inference [16]. This method constructs a tree, whose leaf nodes contain locally active Gaussian process models with a maximum number $\bar{N} \in \mathbb{N}$ of training samples. Given a tree consisting only of the root node and no training samples, a binary tree is iteratively constructed with incoming training data (\mathbf{x}, y) using the following procedure:

- 1) Given a new training pair (\mathbf{x}, y) , the tree is traversed until a leaf is reached by going to the child of node n , which is sampled from a Bernoulli distribution with probability $p_n(\mathbf{x})$.
- 2) If the leaf contains fewer than \bar{N} training pairs continue with 5), else go to 3)
- 3) add two child nodes to the current leaf node n and distribute its training data by sampling from $p_n(\mathbf{x}^{(i)})$ for all $i = 1, \dots, \bar{N}$.
- 4) Go to the child node sampled from $p_n(\mathbf{x})$.
- 5) Add the training pair (\mathbf{x}, y) to the local GP model in the current leaf node and update its hyperparameters.

In this procedure, the Bernoulli distributions with probability functions $p_n(\cdot)$ define the regions where local models are active. In order to quickly determine the probabilities $p_n(\mathbf{x})$, saturating linear functions of the form

$$p_n(\mathbf{x}) = \begin{cases} 0 & \text{if } x_{j_n} < s_n - \frac{o_n}{2} \\ \frac{x_{j_n} - s_n}{o_n} + \frac{1}{2} & \text{if } s_n - \frac{o_n}{2} \leq x_{j_n} \leq s_n + \frac{o_n}{2} \\ 1 & \text{if } s_n + \frac{o_n}{2} < x_{j_n} \end{cases} \quad (6)$$

have been proposed [16], where j_n denotes the dimension in which the state space is split, s_n denotes the value of the splitting plane, and o_n corresponds to the size of the region where both local GPs are active to ensure a smooth global model. The splitting dimension j_n can be chosen, e.g., as the dimension with the maximum spread in the training data, while a simple choice for the position of the splitting plane s_n is the mean of the data in dimension j_n . Finally, the size of the overlapping region o_n is typically chosen to be fixed ratio of the extension the local models.

In order to retain a low computational complexity in the hyperparameter optimization in step 5), we merely perform a single gradient-based optimization step of the log-likelihood, whose partial derivatives are given by

$$\frac{\partial}{\partial \theta_i} \log p(\mathbf{y} | \mathbf{X}, \boldsymbol{\theta}) = \frac{1}{2} \left(\mathbf{y}^T \tilde{\mathbf{K}} \frac{\partial \mathbf{K}}{\partial \theta_i} \tilde{\mathbf{K}} \mathbf{y} - \text{tr} \left(\tilde{\mathbf{K}} \frac{\partial \mathbf{K}}{\partial \theta_i} \right) \right). \quad (7)$$

Hence, hyperparameters are adapted online in step 5) using update rules of the form

$$\tilde{\boldsymbol{\theta}}^{n+1} = \tilde{\boldsymbol{\theta}}^n + \boldsymbol{\psi} \left(\nabla_{\tilde{\boldsymbol{\theta}}} \log p(\mathbf{y} | \mathbf{X}, \boldsymbol{\phi}(\tilde{\boldsymbol{\theta}})) \right) \Delta_t \quad (8)$$

where the step width $\Delta_t \in \mathbb{R}_+$ and the direction function $\boldsymbol{\psi} : \mathbb{R}^p \rightarrow \mathbb{R}^p$ can be defined to realize commonly used optimization schemes, e.g., steepest ascent or conjugate gradient [17]. Since the computational complexity of the update step (8) only depends on the number of training samples in a local model but is independent of the overall amount of data, the update complexity of LoG-GPs remains logarithmic with this online hyperparameter adaptation scheme.

Based on the constructed binary tree, the predictions of local GP models can be efficiently aggregated. For this purpose, given a test point \mathbf{x} , the probabilities $p_m(\mathbf{x})$ along a branch of the tree are multiplied to obtain the weight $w_m(\mathbf{x})$ of leaf node m . Then, standard aggregation schemes such as mixtures of experts [18]

$$\tilde{\mu}(\mathbf{x}) = \sum_{m=1}^M w_m(\mathbf{x}) \mu_m(\mathbf{x}) \quad (9)$$

where M denotes the number of leaf nodes, can be employed to calculate the aggregated mean $\tilde{\mu}(\mathbf{x})$. Since the probabilities $p_n(\cdot)$ are usually chosen such that only few local models are active at the same test point, the tree structure can be again exploited for computing the weights $w_m(\mathbf{x})$, yielding a $\mathcal{O}(\log^2(N))$ complexity for the computation of predictions under weak assumptions [16]. Thereby, LoG-GPs can achieve the high prediction and update rates as required for learning in many control loops.

IV. INDIVIDUALIZED CONTROL USING GAUSSIAN PROCESS BASED ONLINE LEARNING

In order to allow for an individualized treatment of patients, it is necessary to infer personalized models. Even though these models could be learned offline using data

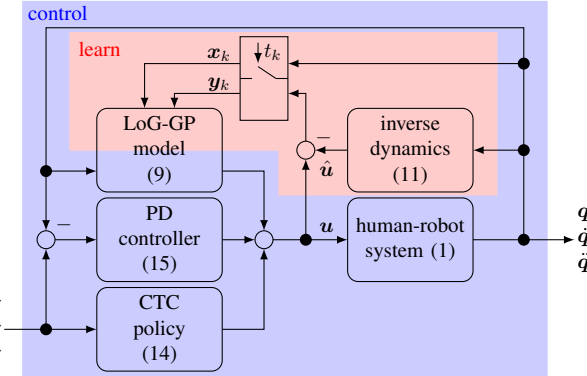


Fig. 1. Online learning control architecture with control components highlighted in blue and learning blocks illustrated in red. Noisy measurements of the system outputs and torque errors $\hat{u} - u$ are taken at times t_k and used to infer a model online using LoG-GPs. Predictions of the LoG-GPs are employed as feedforward term in a CTC control law.

obtained during calibration phases conducted before the actual rehabilitation exercises, this is often perceived as cumbersome by patients. Therefore, we propose an online learning control law based on LoG-GPs which achieves an adaptation to individual patients in virtually real-time.

The proposed control architecture consisting of the online data generation and model inference as well as the feedforward and feedback control components is outlined in Fig. 1. Detailed information about the learning procedure can be found in Section IV-A, while explanations regarding the individualized control law are provided in Section IV-B.

A. Online Data Generation and Model Inference

In order to account for the individual human-induced dynamics in the controller, it is necessary to infer a model online from data. In an idealized scenario, direct measurements of the torques generated by humans would be measured, i.e., $\mathbf{y} = \mathbf{f}_i(\mathbf{x})$, such that a model of the patient's dynamics can be learned from the training samples \mathbf{x}, \mathbf{y} . However, due to the considered lack of force torque sensors for measuring the interaction forces as stated in Assumption 2, we cannot directly employ measurements of $\mathbf{f}_i(\cdot)$ for training GP models. This problem can straightforwardly be overcome by rearranging (1), such that

$$f_i(\mathbf{x}) = \mathbf{u} - \hat{\mathbf{u}}(\mathbf{x}), \quad (10)$$

where

$$\hat{\mathbf{u}}(\mathbf{x}) = \mathbf{H}(\mathbf{q})\ddot{\mathbf{q}} + \mathbf{C}(\mathbf{q}, \dot{\mathbf{q}})\dot{\mathbf{q}} + \mathbf{g}(\mathbf{q}) \quad (11)$$

denotes the inverse dynamics model. Since the applied torque \mathbf{u} is determined by the employed control law and the parameters of the Euler-Lagrange system describing the robot dynamics are known as stated in Assumption 1, $\hat{\mathbf{u}}(\mathbf{x})$ can directly be computed. Therefore, it remains to define a sampling rate $1/\tau$, $\tau \in \mathbb{R}_+$ at which measurements of \mathbf{x} and \mathbf{u} are taken, such that a training data set

$$\{(\mathbf{x}^{(k)} = \mathbf{x}(k\tau), \mathbf{y}^{(k)} = \mathbf{u}(k\tau) - \hat{\mathbf{u}}(\mathbf{x}(k\tau)))\}_{k=0}^K \quad (12)$$

for $K = \lfloor t/\tau \rfloor$ is aggregated based on the online measurements. Using these online data, we can update an independent GP for each target dimension of $\mathbf{y}^{(k)}$, i.e., for each

$i = 1, \dots, d$ a LoG-GP is updated using a training pair $(\mathbf{x}^{(k)}, \mathbf{y}_i^{(k)})$ as explained in Section III-B. In order to employ these LoG-GPs in the control loop, their predictions are concatenated into the vector $\tilde{\mathbf{u}}(\mathbf{x}) = [\mu_1(\mathbf{x}) \dots \mu_d(\mathbf{x})]^T$.

Remark 2: The proposed approach for learning a model of the individual patient dynamics in physical human-robot interaction online is independent of a particular control law. Therefore, the choice of a particular control law does not affect the model inference approach.

B. Individualized Control Law

By exploiting the online learned model in the form of a feedforward control, it is straightforward to achieve a flexible adaptation to the individual dynamics of each patient without the need for additional calibration phases. Therefore, we propose the individualized control law

$$\mathbf{u} = \mathbf{u}_{\text{CTC}}(\mathbf{p}) + \mathbf{u}_{\text{PD}}(\mathbf{e}, \dot{\mathbf{e}}) + \tilde{\mathbf{u}}(\mathbf{x}), \quad (13)$$

where the computed torque control

$$\mathbf{u}_{\text{CTC}}(\mathbf{p}, \mathbf{p}_{\text{ref}}) = \mathbf{H}(\mathbf{q})\ddot{\mathbf{q}}_{\text{ref}} + \mathbf{C}(\mathbf{q}, \dot{\mathbf{q}})\dot{\mathbf{q}}_{\text{ref}} + \mathbf{g}(\mathbf{q}) \quad (14)$$

is used to compensate the nonlinear dynamics of the robotic system, and the PD controller

$$\mathbf{u}_{\text{PD}}(\mathbf{e}, \dot{\mathbf{e}}) = -\mathbf{K}_p \mathbf{e} - \mathbf{K}_d \dot{\mathbf{e}} \quad (15)$$

with control gains $\mathbf{K}_p, \mathbf{K}_d \in \mathbb{R}^{d \times d}$ ensures the convergence of the tracking error $\mathbf{e} = \mathbf{q} - \mathbf{q}_{\text{ref}}$ to a neighborhood of 0.

The PD gains allow a flexible trade-off between compliant behavior and high tracking accuracy, with low gains $\mathbf{K}_p, \mathbf{K}_d$ leading to small control inputs of the PD controller (15) in practice. Since the computed torque control (14) is practically bounded under Assumption 3 and the magnitude of LoG-GP predictions is restricted through the observed torques [19], which are applied by the patient, it is straightforward to see that the individualized control law (13) with a sufficiently compliant PD controller can ensure safe interaction forces. This dependency of safety on the control gains is demonstrated experimentally in Section V-B.

Remark 3: Since the individualized control law (13) is based on a classical computed torque approach and uniform error bounds for predictions with LoG-GPs can be shown under weak assumptions [16], it is straightforward to analyze the stability of the closed-loop human-robot system using Lyapunov theory analogously to, e.g., [20], [21]. For reasons of brevity, a formal stability analysis is omitted here.

V. EXPERIMENTAL EVALUATION

For the evaluation of the proposed learning-based controller, we perform experiments with a two DoF human-robot interaction setup, which is explained in Section V-A. First, the capacity of the method to successfully assist during a rehabilitation exercise whilst applying safe control outputs is shown in Section V-B. After this initial validation, the method is contrasted with a controller tuned for one individual, in Section V-C. Thereby, we demonstrate the learners ability to adapt to different human operators and provide personalized assistance.

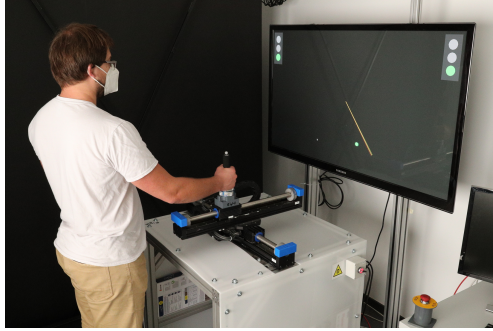


Fig. 2. Reenactment of an individual performing the experiment task with the manipulandum. Consent for the publication of the image was obtained.

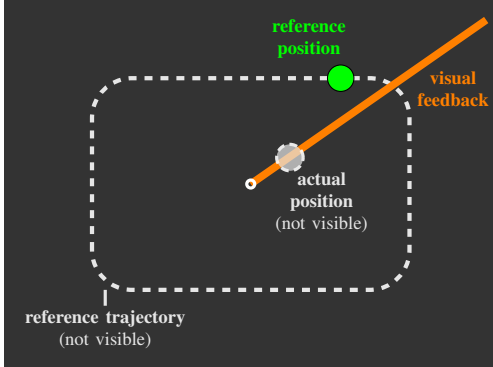


Fig. 3. Exemplary depiction of the task design. The rounded rectangle drawn with the gray, dashed line represents the reference trajectory of the green circle, which the participant is instructed to track. Instead of the actual current position, depicted by the gray circle, the subject can only

A. Experiment Setup and Task Design

The experiments are executed on a two DoF manipulandum, which consists of two orthogonally mounted single rail stages (Copley Controls Thrustube Module), each driven by linear servo motors. Both rail stages are equipped with optical encoders that measure the position of a cart on the upper rail with $1\text{ }\mu\text{m}$ precision. Additionally, a six DoF force-torque sensor (JR3-75M25) is mounted below the handle, through which the human interacts with the system, to measure forces in the horizontal plan. The force-torque sensor is strictly required to operate the device and is not used for the computation of control policies. Additionally, an inherent output force limitation is integrated as a safety measure, which guarantees that the interaction force applied to the human remains in safe regions, therefore, enabling experiments with aggressively tuned controllers. The device runs at 4 kHz and the workspace of the complete apparatus spans $\pm 0.20\text{ m}$ in both DoF. Visual feedback to perform the task is provided to the user through a screen placed behind the apparatus. The complete experiment setup and apparatus is shown in Fig. 2. The task itself is designed as follows:

Standing in front of the apparatus and facing the screen, the subjects are instructed to track a green dot by moving the handle on top of the cart. In addition the participants are informed that different controllers will support them during task execution. Since the experiments are performed by healthy subjects, the provided visual feedback is artificially modified, therefore, limiting the participants' ability

TABLE I
PD CONTROL GAINS USED IN THE EXPERIMENTS.

	LOW GAIN	HIGH-GAIN	GP	TUNED GAINS
k_p	1	600	1	35
k_d	0.1	60	0.1	3.5

to successfully perform the task and thereby mimicking the physical limitations of an impaired patient. Specifically, the subjects do not see their current position in the task space entirely, but instead only the angle from the origin is visualized through a pointer. However, despite the limited feedback, their tracking performance is still evaluated on the position error in Cartesian coordinates. The task design and the visual feedback is depicted in Fig. 3. Each run of the experiment begins at the same starting position for the green circle and consists of five repetitions of the reference trajectory. The complete experimental procedure can be split into two parts; first a training phase, followed by a test phase. During the initial training phase the participants get accustomed to the task and the assistance by performing one experiment run with each controller. Subsequently, the test phase begins, which consists of four experiment runs per controller. At every run a random controller variation is selected for assistance. If during any trial the workspace limit is reached, the device shuts down as a safety precaution and the run is evaluated as a failure. The failed runs are not repeated subsequently.

B. Compliance and Accuracy with Learning Control

In order to demonstrate the applicability of our approach, we conduct a user study with 9 healthy, right-handed participants between the age of 22 and 35. Participants signed a written informed consent, approved by the ethics committee of the medical faculty of the Technical University of Munich. During the experiment the operators perform a task whilst being assisted by three different variations of the proposed control architecture. A high-gain, low-gain and GP variation with PD control-parametrization according to Table I and diagonal gain matrices $\mathbf{K}_p = k_p \mathbf{I}$, $\mathbf{K}_d = k_d \mathbf{I}$, $k_p, k_d \in \mathbb{R}_+$. For the high-gain and low-gain controller there is no learning GP and they only differ with regards to the gains used for the PD controller (15). Differently, the GP controller uses the individualized control law (13) including the proposed learning-based controller with small gains for the PD controller. The online hyperparameter adaptation (8) is realized using RPROP [22] since it has been demonstrated to exhibit lower computational complexity and faster convergence compared to other gradient-based optimization schemes [23]. All three controllers have the same CTC policy (14) and the GP runs at a update and prediction rate of 200 Hz, resulting in approximately 10000 training samples at the end of one experimental run.

The analysis of the experimental results are shown in Fig. 4. The top bar plots depict the tracking performance by comparing the mean and standard deviation of the summed absolute error for each controller. It is clearly visible that the low-gain controller leads to the worst tracking accuracy and exhibits a notable variation between subjects, which is appar-

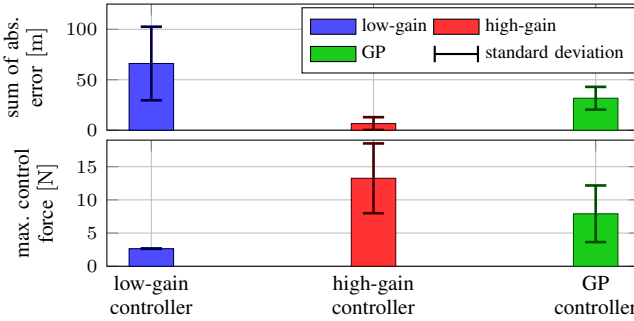


Fig. 4. Top: Mean and standard deviation of the summed absolute error for all participants over low-gain, high-gain and GP controller configuration. Bottom: Mean and standard deviation of the maximum applied control force norm at each run. The GP controller trades-off applied maximum control force and tracking performance, while the low-gain and high-gain controller either exhibit low tracking performance or overly large control forces.

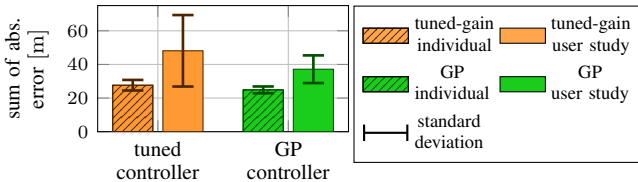


Fig. 5. Mean and standard deviation of the summed absolute error for one surrogate participant and the complete user study. While the tuned PD controller and GP controller perform comparably for the surrogate individual, only the GP controller adapts in the user study to personalize the assistance required for acceptable tracking performance.

ent due to the large standard deviation. In fact, four subjects reached the workspace limit at least once when they were assisted by the low-gain controller, resulting in a total of eight failed runs, which demonstrates the issues of highly compliant controllers in ensuring a successful task execution. Since the failed runs are particularly short they are not included in the analysis depicted in Fig. 4. While the high gain controller does not suffer from failed trials and exhibits the best control performance, it can result in uncomfortable interaction forces, which may ultimately become unsafe. This can be observed at the bottom of Fig. 4 depicting the applied maximum forces, which are largest for the high gain configuration. In contrast to these PD control laws, the proposed online learning controller adapts itself to each participant. Since the labels used during training of the GP correspond to the human-generated torques, it is highly unlikely that higher control forces are generated than the human operator can manage. This is also demonstrated by the experiments as shown in Fig. 4. The applied maximum control forces of the GP controller remain significantly smaller compared to the high-gain configuration, while the tracking performance is strongly improved over the low-gain controller. Therefore, it is demonstrated that the proposed online learning control scheme is capable of successful task execution while being safer than high-gain controllers due to smaller interaction forces.

C. Personalized Assistance through Online Learning

In order to demonstrate the benefits of the proposed learning controller, we compare it to a PD controller with tuned gains. Due to the lack of a better procedure for adaptation in human-robot interaction, the gains of the PD controller

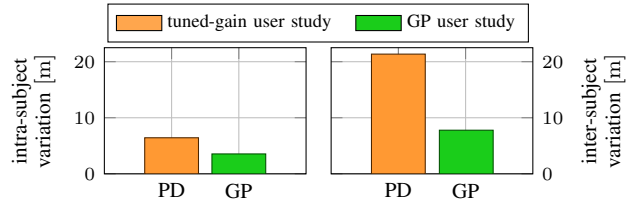


Fig. 6. Left: Average of intra-subject standard deviation in tracking error. Right: Inter-subject standard deviation of participant specific average tracking error. The adaptability of the GP controller is reflected in the smaller intra- and inter-subject variation.

are tuned heuristically to balance the applied forces and the resulting tracking performance. As practical considerations prevent a tuning with all participants, one individual is chosen instead. However, since the PD controller needs to be safe for all users, a cautious tuning is preferred, which tends to result in lower control gains. The best trade-off is obtained for the parametrization depicted on the right side of Table I.

The tuned PD controller and the proposed online learning control law are evaluated as described in Section V-B, which leads to the results depicted in Fig. 5. For the individual, the two controllers perform comparably well with regards to tracking performance, with the GP controller leading to slightly better tracking. However, the observed difference in tracking error is insignificant, since it lies within the statistical variation, and can be attributed to the cautious tuning of the PD controller. When deploying the tuned PD controller to previously unobserved individuals and comparing the performance to the learning-based GP controller in a user study, it can be seen that the tuned PD controller performs significantly worse. Similarly, the GP controller on average results in higher tracking errors in the user study than for the surrogate individual. However, the increase in mean tracking error is larger for the tuned PD controller with a substantial growth in the standard deviation. Therefore, the tuned PD controller leads to inconsistent tracking results, which can be attributed to the different levels of task proficiency of the participants. This becomes even clearer when looking at the intra- and inter-subject variation of the tracking error as depicted in Fig. 6. While the participants exhibit a similar variation of the tracking error among the experiment runs for both controllers, the variation of the tracking error between different subjects is significantly larger for the tuned PD controller. This is due to the inability of the PD control law to adapt to unproficient participants, which require more guidance to execute the task properly. In contrast, the GP controller provides personalized support for each subject, such that the variation between different participants can be reduced.

VI. CONCLUSION

This paper introduces a novel online learning control method for personalized rehabilitation robotics. This is the first time that GPs are used directly in the control loop during physical human-robot collaboration. Furthermore, the proposed method facilitates personalized assistance via online learning with previously unseen update rates. The approach is validated in an experimental user study, which confirms the adaptation capabilities of the learning-based controller.

REFERENCES

[1] V. L. Feigin, M. H. Forouzanfar, R. Krishnamurthi, G. A. Mensah, M. Connor, D. A. Bennett, A. E. Moran, R. L. Sacco, L. Anderson, T. Truelsen, M. O'Donnell, N. Venketasubramanian, S. Barker-Collo, C. M. Lawes, W. Wang, Y. Shinohara, E. Witt, M. Ezzati, and M. Naghavi, "Global and regional burden of stroke during 1990-2010: Findings from the Global Burden of Disease Study 2010," *The Lancet*, vol. 383, no. 9913, pp. 245-255, 2014. [Online]. Available: <https://pubmed.ncbi.nlm.nih.gov/24449944/>

[2] P. A. Ringleb, M. G. Bousser, G. Ford, P. Bath, M. Brainin, V. Caso, Á. Cervera, A. Chamorro, C. Cordonnier, L. Csiba, A. Davalos, H. C. Diener, J. Ferro, W. Hacke, M. Hennerici, M. Kaste, P. Langhorne, K. Lees, D. Leyls, J. Lodder, H. S. Markus, J. L. Mas, H. P. Mattle, K. Muir, B. Norrving, V. Obach, S. Paolucci, E. B. Ringelstein, P. D. Schelling, J. Sivenius, V. Skvortsova, K. S. Sunnerhagen, L. Thomassen, D. Toni, R. Von Kummer, N. G. Wahlgren, M. F. Walker, and J. Wardlaw, "Guidelines for management of ischaemic stroke and transient ischaemic attack 2008," pp. 457-507, 2008. [Online]. Available: <https://pubmed.ncbi.nlm.nih.gov/18477843/>

[3] H. I. Krebs, J. J. Palazzolo, L. Dipietro, M. Ferraro, J. Krol, K. Rannekleiv, B. T. Volpe, and N. Hogan, "Rehabilitation robotics: Performance-based progressive robot-assisted therapy," *Autonomous Robots*, vol. 15, no. 1, pp. 7-20, 2003.

[4] Y. Yang, L. Wang, J. Tong, and L. Zhang, "Arm rehabilitation robot impedance control and experimentation," in *2006 IEEE International Conference on Robotics and Biomimetics, ROBIO 2006*, 2006, pp. 914-918.

[5] J. Zhang and C. C. Cheah, "Passivity and Stability of Human-Robot Interaction Control for Upper-Limb Rehabilitation Robots," *IEEE Transactions on Robotics*, vol. 31, no. 2, pp. 233-245, 2015.

[6] X. Li, Y. H. Liu, and H. Yu, "Iterative learning impedance control for rehabilitation robots driven by series elastic actuators," *Automatica*, vol. 90, no. April, pp. 1-7, 2018.

[7] F. Just, O. Özen, P. Bösch, H. Bobrovsky, V. Klamroth-Marganska, R. Riener, and G. Rauter, "Exoskeleton transparency: Feed-forward compensation vs. disturbance observer," *at - Automatisierungstechnik*, vol. 66, pp. 1014-1026, 11 2018.

[8] C. An and J. Hollerbach, "Dynamic stability issues in force control of manipulators," in *Proceedings. 1987 IEEE International Conference on Robotics and Automation*, vol. 4, 1987, pp. 890-896.

[9] W. He, S. S. Ge, Y. Li, E. Chew, and Y. S. Ng, "Neural Network Control of a Rehabilitation Robot by State and Output Feedback," *Journal of Intelligent and Robotic Systems: Theory and Applications*, vol. 80, no. 1, pp. 15-31, 2015.

[10] J. R. Medina, H. Börner, S. Endo, and S. Hirche, "Impedance-Based Gaussian Processes for Modeling Human Motor Behavior in Physical and Non-Physical Interaction," *IEEE Transactions on Biomedical Engineering*, vol. 66, no. 9, pp. 2499-2511, 2019.

[11] P. Beckerle, G. Salvietti, R. Unal, D. Prattichizzo, S. Rossi, C. Castellini, S. Hirche, S. Endo, H. B. Amor, M. Ciocarlie, F. Mastrogianni, B. D. Argall, and M. Bianchi, "A human-robot interaction perspective on assistive and rehabilitation robotics," *Frontiers in Neurorobotics*, vol. 11, no. MAY, pp. 1-6, 2017.

[12] J. Hollerbach, W. Khalil, and M. Gautier, "Model Identification," in *Springer Handbook of Robotics*, B. Siciliano and O. Khatib, Eds. Springer Berlin Heidelberg, 2008, ch. 14, pp. 321-344.

[13] C. E. Rasmussen and C. K. I. Williams, *Gaussian Processes for Machine Learning*. Cambridge, MA: The MIT Press, 2006.

[14] D. Nguyen-Tuong and J. Peters, "Incremental sparsification for real-time online model learning," *Journal of Machine Learning Research*, vol. 9, pp. 557-564, 2010.

[15] D. Nguyen-Tuong, M. Seeger, and J. Peters, "Model learning with local Gaussian process regression," *Advanced Robotics*, vol. 23, no. 15, pp. 2015-2034, 2009.

[16] A. Lederer, A. Odomez Conejo, K. Maier, W. Xiao, J. Umlauft, and S. Hirche, "Gaussian Process-Based Real-Time Learning for Safety Critical Applications," in *International Conference on Machine Learning*, 2021, pp. 6055-6064.

[17] P. Pedregal, *Introduction to Optimization*. New York, NY: Springer Science+Business Media, 2004.

[18] V. Tresp, "Mixtures of Gaussian processes," *Advances in Neural Information Processing Systems*, 2001.

[19] A. Capone, A. Lederer, and S. Hirche, "Gaussian Process Uniform Error Bounds with Unknown Hyperparameters for Safety-Critical Applications," 2021. [Online]. Available: <http://arxiv.org/abs/2109.02606>

[20] M. K. Helwa, A. Heins, and A. P. Schoellig, "Provably Robust Learning-Based Approach for High-Accuracy Tracking Control of Lagrangian Systems," *IEEE Robotics and Automation Letters*, vol. 4, no. 2, pp. 1587-1594, 2019.

[21] J. Umlauft and S. Hirche, "Feedback Linearization based on Gaussian Processes with event-triggered Online Learning," *IEEE Transactions on Automatic Control*, vol. 65, no. 10, pp. 4154-4169, 2019.

[22] M. Riedmiller and H. Braun, "A Direct Adaptive Method for Faster Backpropagation Learning: The RPROP Algorithm," in *IEEE International Conference on Neural Networks*, 1993, pp. 586-591.

[23] M. Blum and M. Riedmiller, "Optimization of gaussian process hyperparameters using Rprop," in *European Symposium on Artificial Neural Networks, Computational Intelligence and Machine Learning*, 2013, pp. 339-344.